AD-A171 133 A RUBIDIUM CLOCK MODEL(U) AEROSPACE CORP EL SEGUNDO CA 1/1
CHEMISTRY AND PHYSICS LAB R P FRUEHOLZ ET AL.
15 JUN 86 TR-0086(6945-05)-3 SD-TR-86-41
UNCLASSIFIED F04701-85-C-0086 F/G 14/2 NL

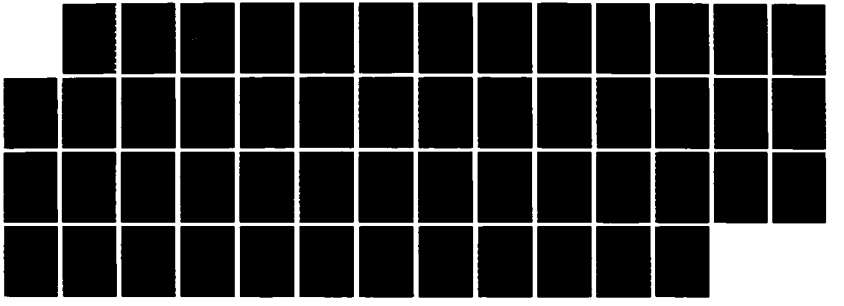

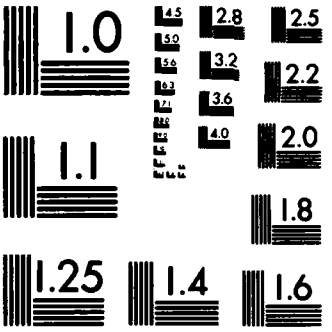

MICROCOPY RESOLUTION TEST CHART
NATIONAL BUREAU OF STANDARDS-1963-A

REPORT SD-TR-86-41

(12)

A Rubidium Clock Model

R. P. FRUEHOLZ and J. C. CAMPARO
Chemistry and Physics Laboratory
Laboratory Operations
The Aerospace Corporation
El Segundo, CA 90245

15 June 1986

Prepared for

SPACE DIVISION
AIR FORCE SYSTEMS COMMAND
Los Angeles Air Force Station
P.O. Box 92960, Worldway Postal Center
Los Angeles, CA 90009-2960

This report was submitted by The Aerospace Corporation, El Segundo, CA 90245, under Contract No. F04701-85-C-0086 with the Space Division, P.O. Box 92960, Worldway Postal Center, Los Angeles, CA 90009-2960. It was reviewed and approved for The Aerospace Corporation by S. Feuerstein, Director, Chemistry and Physics Laboratory.

Capt Matthew Hanson/YEZ was the project officer for the Mission-Oriented Investigation and Experimentation (MOIE) Program.

This report has been reviewed by the Public Affairs Office (PAS) and is releasable to the National Technical Information Service (NTIS). At NTIS, it will be available to the general public, including foreign nationals.

This technical report has been reviewed and is approved for publication. Publication of this report does not constitute Air Force approval of the report's findings or conclusions. It is published only for the exchange and stimulation of ideas.

12 May 86

MATTHEW HANSON, Capt, USAF
MOIE Project Officer
SD/YEZ

JOSEPH HESS, GM-15
Director, AFSTC West Coast Office
AFSTC/WCO OL-AB

UNCLASSIFIED

SECURITY CLASSIFICATION OF THIS PAGE (When Data Entered)

AD-A171 133

REPORT DOCUMENTATION PAGE

READ INSTRUCTIONS BEFORE COMPLETING FORM

1. REPORT NUMBER: SD-TR-86-41	2. GOVT ACCESSION NO.
3. RECIPIENT'S CATALOG NUMBER	
4. TITLE (and Subtitle): A RUBIDIUM CLOCK MODEL	5. TYPE OF REPORT & PERIOD COVERED
6. PERFORMING ORG. REPORT NUMBER: TR-0086(6945-05)-3	
7. AUTHOR(s): Robert P. Frueholz and James C. Camparo	8. CONTRACT OR GRANT NUMBER(s): F04701-85-C-0086
9. PERFORMING ORGANIZATION NAME AND ADDRESS: The Aerospace Corporation, El Segundo, Calif. 90245	10. PROGRAM ELEMENT, PROJECT, TASK AREA & WORK UNIT NUMBERS
11. CONTROLLING OFFICE NAME AND ADDRESS: Space Division, Los Angeles Air Force Station, Los Angeles, Calif. 90009-2960	12. REPORT DATE: 15 June 1986
	13. NUMBER OF PAGES: 47
14. MONITORING AGENCY NAME & ADDRESS (if different from Controlling Office)	15. SECURITY CLASS. (of this report): Unclassified
	15a. DECLASSIFICATION/DOWNGRADING SCHEDULE

16. DISTRIBUTION STATEMENT (of this Report)

Approved for public release; distribution unlimited.

17. DISTRIBUTION STATEMENT (of the abstract entered in Block 20, if different from Report)

18. SUPPLEMENTARY NOTES

19. KEY WORDS (Continue on reverse side if necessary and identify by block number)

Atomic Clocks
Noise Processes
Rubidium Frequency Standard

20. ABSTRACT (Continue on reverse side if necessary and identify by block number)

In this report, a signal model for the rubidium (Rb) clock, is developed. This model combines feedback analysis of the clock's servo-control circuitry with the atomic physics required to describe the processes occurring within the Rb absorption cell. The model permits clock performance, in terms of Allan variance, to be predicted from a number of electronic and physical parameters. While building on prior studies of Rb standards, the model incorporates a number of features which make it distinctive.

DD FORM 1473 FACSIMILE

UNCLASSIFIED

SECURITY CLASSIFICATION OF THIS PAGE (When Data Entered)

19. KEY WORDS (Continued)

20. ABSTRACT (Continued)

All previous models of the Rb clock were limited to an analysis of the clock's short-term performance, Allan variance averaging times of less than 10,000 sec. However, by explicitly including the effects of discharge lamp intensity fluctuations, which are transformed into output frequency variations via the light shift effect, clock performance can be predicted for averaging times greater than 10,000 sec. Furthermore, the model is the first which incorporates the influence of an optically thick Rb vapor along with the diffusion of optically pumped atoms to the walls of the absorption cell into the calculation of clock performance. In addition, the model has been developed in sufficient generality to permit its application to diode laser pumped clocks using other alkali metals.

As part of our validation of the model, it is checked against experimental results from a recent test of a prototype Rb clock manufactured by the EG&G, Corporation Electronic Components Division. Agreement between measured and predicted Allan variances for both short and long averaging time periods is excellent.

PREFACE

The authors wish to thank L. G. Redekopp of the University of Southern California for aid in evaluating the contour integrals.

CONTENTS

PREFACE..... 1

I. INTRODUCTION..... 9

II. ANALYSIS..... 13

A. Feedback Analysis of Servo Control Circuitry..... 13

B. Atomic System Analysis..... 18

C. Integration of Atomic Physics with Feedback Analysis..... 28

III. MODEL VERIFICATION..... 31

IV. CONCLUSIONS AND SUMMARY..... 43

REFERENCES..... 47

APPENDIX: RESULTS OF COMPLEX CONTOUR INTEGRATION..... 51

FIGURES

1. Schematic Diagram of a Passive Rubidium Gas Cell Frequency Standard and Energy Level Diagram of Rb^{87} Exhibiting the Radiative Transitions of Interest..... 10

2. Block Diagram of the Gas Cell Frequency Standard Employed in Servo-Loop Feedback Analysis..... 14

3. Global Fractional Population ζ in the $F = b = I - 1/2$ Hyperfine Multiplet as a Function of Resonance Cell Temperature for the Case of Optical Pumping Out of Only This Multiplet..... 33

4. The Measure of Hyperfine Polarization $\langle \hat{I} \cdot \hat{S} \rangle$ has an Axial Spatial Distribution That is Temperature Dependent..... 34

5. Optically Detected Hyperfine Transition Lineshape..... 37

6. Frequency Stability of the EG&G Rb Gas Cell Frequency Standard in Terms of Allan Variance $\sigma_y(\tau)$..... 40

7. Calculated Allan Variance $\sigma_y(\tau)$ for Passive Rb^{87} Gas Cell Standard for Two Control Loop Attack Times..... 42

8. Short-Term Allan Variance Slope for the Parameters of Table 1 as a Function of Microwave Rabi Frequency, or Equivalently, Microwave Power Fed into the Cavity Assuming a Q = 100..... 44

TABLES

1. Parameters for Clock Signal Model..... 35

2. Comparison of Predicted Clock Performance with Measured Clock Performance..... 39

I. INTRODUCTION

The passive Rb gas cell atomic clock is presently the most often used atomic frequency standard in high-performance systems because of its particular advantages of small size, low weight, low power consumption, and excellent short-term performance. In this standard the Rb^{87} atomic resonance frequency associated with the hyperfine ground state splitting is used as a reference to control the frequency of a quartz crystal oscillator (see Fig. 1 and Ref. 1). Servo control circuitry is used to transfer the stability of the microwave atomic transition to the crystal oscillator, and for times greater than the time constant of the feedback loop, the crystal oscillator frequency stability reflects that of the atomic system. The Rb hyperfine resonance is optically detected using the standard technique of optical pumping double resonance, where the source of optical pumping radiation is typically a Rb^{87} discharge lamp. For effective optical pumping, the output of the discharge lamp is filtered by transmission through a vapor of Rb^{85} atoms. The filtering may be carried out using a discrete separated filter cell (SFC), as is shown in Fig. 1, or by combining the filter and absorption cells into an integrated filter cell (IFC).[1,2] In either case the atomic microwave signal appears at a photodiode as a small light intensity modulation component resting on a large DC background. In this report, a nonempirical model of the gas cell frequency standard is developed, with the aim of putting the operation and performance of the gas cell clock on a sound theoretical footing.

In past years, a number of other authors have investigated Rb clock performance by developing clock models of varying complexities.[1,3-7] We would be remiss if we did not acknowledge the foundation these studies have provided for our own work. The present model, though, has a number of significant differences from the previous investigations. All previous models were limited to short-term performance analysis, using Allan variance averaging times of less than 10^4sec. During this time regime, shot noise at the photodetector limits clock performance. The current analysis is the first that is valid for times greater than 10^4sec. This was accomplished by

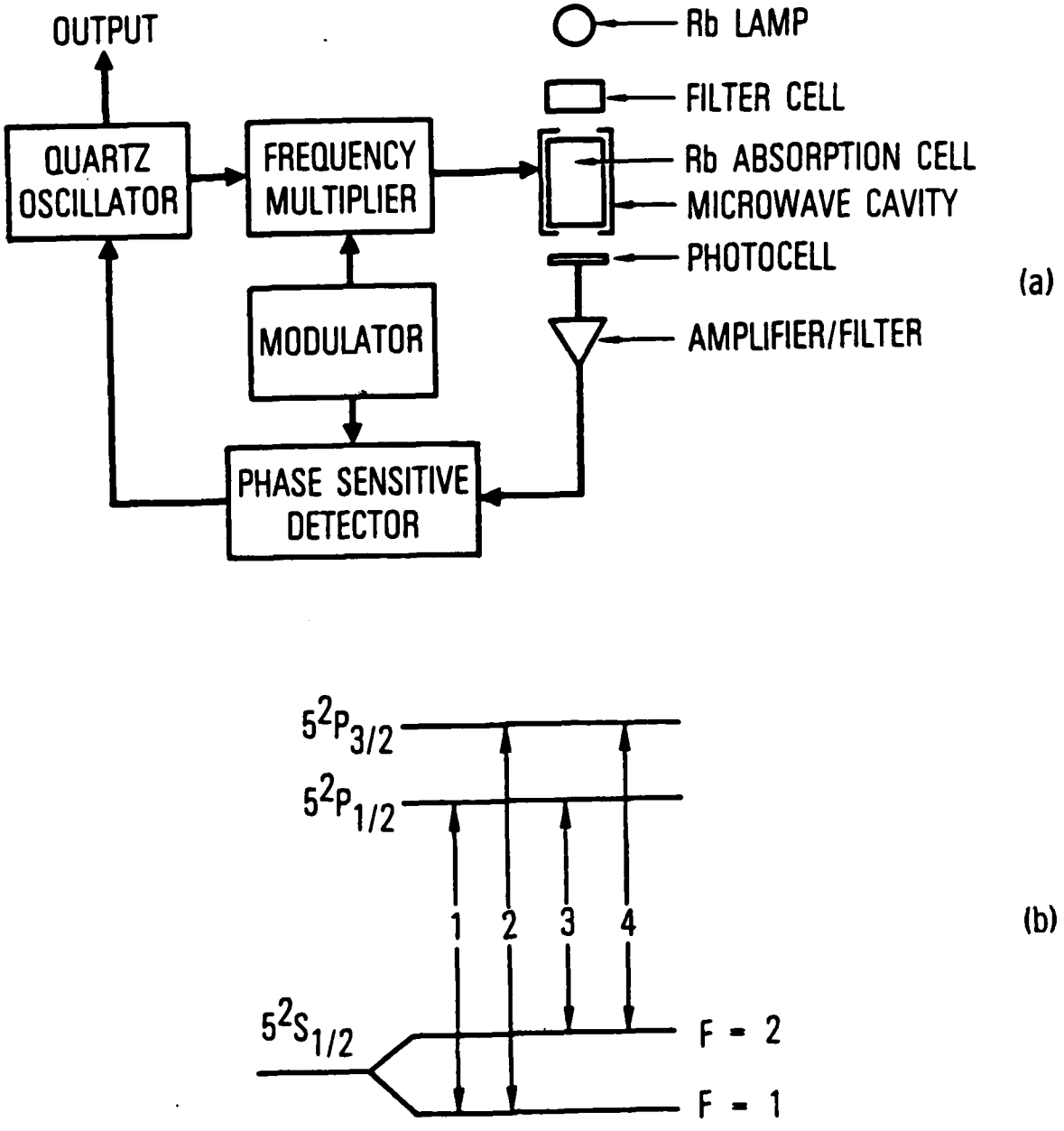

Fig. 1. (a) Schematic Diagram of a Passive Rubidium Gas Cell Frequency Standard; (b) Energy Level Diagram of Rb^{87} Exhibiting the Radiative Transitions of Interest.

explicitly including the effects of discharge lamp intensity fluctuations, which are transferred into output frequency variations via the light-shift effect. Additionally, the model is the first which incorporates the influence of an optically thick Rb vapor along with the diffusion of optically pumped atoms to the walls of the absorption cell into the calculation of clock performance. Inclusion of these processes very dramatically affects the axial Rb hyperfine polarization within the cell and how each segment of the cell contributes to the observed hyperfine resonance signal. With the advent of diode laser sources for optical pumping,[8] practical gas cell clocks based on alkalies other than Rb, e.g., Cs, may be envisioned. Consequently, the current analysis has been carried out for arbitrary nuclear spin, permitting analysis of alternative gas cell clocks.

This report has been divided into several sections. In the analysis section, the feedback analysis of the servo-control loop, along with the physical analysis and computational procedures yielding the Rb hyperfine lineshape, are developed. Integration of these components yields the functioning model. In the model verification section, the validity of the model is established by modeling the performance of a prototype "state-of-the-art" Rb standard[9,10] manufactured by EG&G, Electronic Components Division, for use on NAVSTAR/global positioning system satellites. In the final section, implications of this clock model are discussed along with potential avenues for Rb clock performance improvement.

II. ANALYSIS

A. FEEDBACK ANALYSIS OF SERVO CONTROL CIRCUITRY

The function of the servo control circuitry is to transfer the stability of the microwave atomic transition to the crystal oscillator. The feedback analysis of this system provides a means of understanding how the electronics and the physics package affects clock performance at all analysis times. In Fig. 2 the clock is displayed in a functional block diagram to which standard linear feedback analysis may be applied. The analysis is carried out in the frequency domain, and the inputs are the power spectral densities of the various system noise sources. $S_y^{cr}(f)$ and $S_y^{ph}(f)$ are the spectral densities of the fractional frequency fluctuations of the crystal oscillator and the physics package, respectively.[11] Other authors have carried out most of the required feedback analysis previously.[7,12,13] The spectral density of the fractional frequency fluctuations of the entire clock, voltage controlled quartz crystal oscillator (VCXO) locked to the atomic system, $S_y^{Rb}(f)$, is given by

$$S_y^{Rb}(f) = \frac{(f/f_n)^2}{1 + (f/f_n)^2} S_y^{cr}(f) + \frac{1}{1 + (f/f_n)^2} S_y^{ph}(f) \qquad (1a)$$

with

$$f_n \equiv \frac{MmR\mu}{2\pi t_1} \qquad (1b)$$

where R is the effective impedance of the current to the voltage converter/amplifier, M is the frequency multiplier's multiplication factor, and m is the atomic system response relating a microwave frequency detuning Δf to a detected error signal current i,

$$i = m\,\Delta f \qquad (2)$$

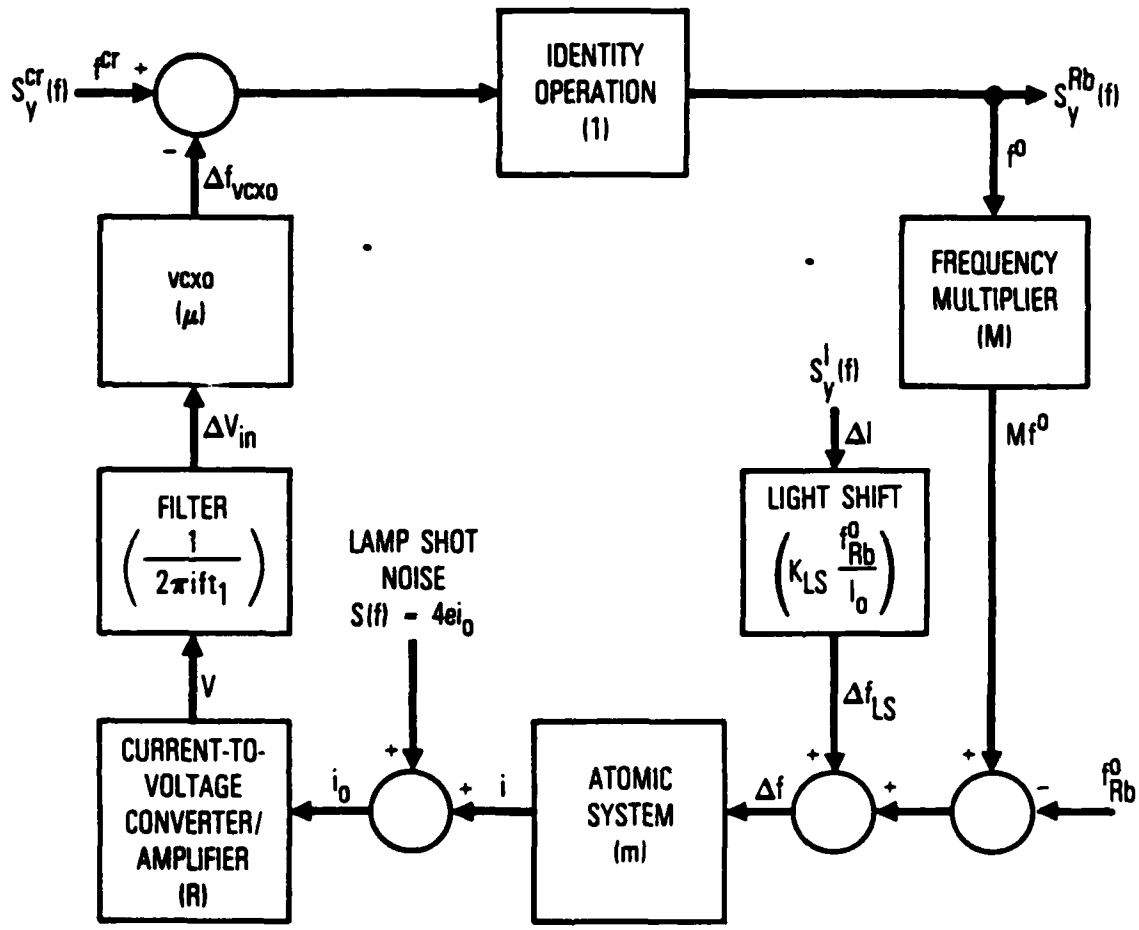

Fig. 2. Block Diagram of the Gas Cell Frequency Standard Employed in Servo-Loop Feedback Analysis. The transfer function of each element is in parentheses.

Effectively, m is found to be the slope of the discriminator pattern, proportional to the second derivative of the Rb hyperfine lineshape evaluated at the Rb resonance's central frequency. This parameter is obtained through modeling of the physics package (see subsections II.B and II.C). The VCXO response μ relates a change in control voltage ΔV_{in} to a change in the crystal's output frequency Δf_{VCXO},

$$\Delta f_{VCXO} = \mu \Delta V_{in} \tag{3}$$

In Eq. (1b), t_1 is the time constant of the integrating filter which has a transfer function of the form $1/(2\pi i f t_1)$. Equation (1a) indicates that the spectral density of the clock's fractional frequency fluctuations for frequencies above f_n is determined by the crystal oscillator and for frequencies below f_n by the physics package. In the time domain, this implies that for times less than the loop attack time ($1/2\pi f_n$), the clock frequency stability is specified by the crystal oscillator; for times greater than the attack time, frequency stability is defined by the atomic system (physics package).

The principal difference between previous analyses and the present one is the explicit inclusion of the effects of the lamp-induced light shift[14,15] of the Rb hyperfine transition frequency. It is clear that lamp intensity fluctuations at frequencies less than f_n are mapped directly into variations of the clock output frequency via the light-shift effect. Recent experimental studies have shown that for the EG&G Rb frequency standard, these light-induced frequency fluctuations specify the long-term frequency stability of the standard.[16] Further, these lamp-induced frequency fluctuations should set a fundamental limitation to the long-term frequency stability of Rb clocks in general. Including the light-shift effect, the physics package's spectral density of fractional frequency fluctuations takes the form

$$S_y^{ph}(f) = \left[K_{LS}^2 \, S_y^I(f) + \frac{4ei_o}{(f_{Rb}^o m)^2}\right] \qquad (4)$$

where the light-shift coefficient K_{LS} relates a change in clock frequency Δf_{LS}, and the nominal clock frequency f_{Rb}^o to a change in light intensity ΔI, and the nominal light intensity I_o

$$\Delta f_{LS} / f_{Rb}^o = K_{LS} \, (\Delta I / I_o)$$

In Eq. (4), $S_y^I(f)$ is the power spectral density of the fractional light intensity $(\Delta I/I_o)$ fluctuations. The second term on the right-hand side of the equation is the result of shot noise at the photodetector, where e is the electronic charge, i_o is the total lamp-induced photocurrent, and f_{Rb}^o is the Rb hyperfine resonance frequency.

Modeling of the physics package supplies i_o, while $S_y^I(f)$ can be experimentally determined from lamp intensity fluctuations recorded as a function of time. Whereas in principle the light-shift coefficient can be calculated from fundamental parameters, in the present analysis an experimentally measured value is used. Equation (4) explicitly indicates how lamp intensity fluctuations and the light shift can impact clock performance. The importance of minimizing the light-shift coefficient as well as the design of lamps yielding extremely stable intensities are apparent.

The spectral density of fractional frequency fluctuations is related to the Allan variance $\sigma_y(\tau)$ via the following integral transformation:[11]

$$\sigma_y^2(\tau) = 2 \int_0^\infty S_y^{Rb}(f) \, \frac{\sin^4(\pi \tau f)}{(\pi \tau f)^2} \, df \qquad (5)$$

where τ is the Allan variance frequency averaging time. For the EG&G Rb frequency standard, $S_y^I(f)$ was of the form[16]

$$S_y^I(f) = A + \frac{B}{f^2} \tag{6}$$

which is the sum of white and random walk contributions. Crystal oscillators display fractional frequency spectral densities of the form [17]

$$S_y^{cr}(f) = \frac{C}{f} + Df + Ef^2 \tag{7}$$

Combining this information with Eq. (2), we observe that the following integrals must be evaluated when obtaining the Allan variance over all averaging times:

$$A(\tau) = \int_0^\infty \frac{f^\alpha}{1 + (f/f_n)^2} \sin^4(\pi\tau f)\, df \tag{8}$$

$$\alpha = -4, -2, -1, 1, 2$$

To permit rapid evaluation of Allan variances, particularly for averaging times near the loop attack time, these integrals were evaluated analytically using complex contours. The results of these evaluations are tabulated in the appendix.

With the evaluation of the integrals, the Allan variance may be readily extracted from the modeled clock's spectral density of fractional frequency fluctuations. This spectral density is a function of crystal and loop parameters as well as inputs describing the performance of the physics package. In the following paragraphs, the analysis applied to the physics package, yielding the total detected photocurrent and the atomic system response, m, is described.

B. ATOMIC SYSTEM ANALYSIS

Figure 1a exhibits the basic physics package elements of an optically pumped gas cell atomic frequency standard: the lamp, the filter cell, the resonance cell, and the photodetector. In combination, the lamp and filter cell produce a spectral emission that preferentially excites atoms in the resonance cell out of one of the $5^2S_{1/2}$ ground state hyperfine multiplets. For example, the optical emission lines corresponding to transitions from $F = 2$ (i.e., transition numbers 3 and 4 in Fig. 1b) may be effectively blocked by the filter cell, so that only those atoms in the $F = 1$ hyperfine multiplet can absorb light. Because an excited atom can decay from the $5^2P_{3/2}$ or $5^2P_{1/2}$ state into either ground state hyperfine multiplet, the successive action of several optical absorptions and reemissions will lead to a transfer of population from one hyperfine multiplet into the other. Furthermore, because this process of optical pumping depopulates the optically absorbing hyperfine multiplet, the equilibrium light intensity transmitted by the resonance cell and detected by the photodiode will be at a maximum. If microwaves of the appropriate frequency, 6835 MHz, are now applied to the cavity, atoms in the overpopulated hyperfine multiplet will be induced into returning to the optically absorbing hyperfine multiplet. This appropriate frequency is then detected as a decrease in the light intensity transmitted by the resonance cell. Because the Q of the atomic interaction with the microwaves is 10^7-10^8, the decrease in transmitted light intensity can be used to discriminate against very small changes in the 6835 MHz microwave frequency.[1]

From the outline of gas cell frequency standard operation presented above, it is clear that an accurate calculation of the response of the transmitted light intensity to variations in the microwave frequency is a primary concern for a model of clock performance. Typically, this problem is approached in one of three directions. Quite often one attempts to describe the atomic system as a two-level atom interacting with the microwaves,[18] an approach that has the advantage of being easy to work with and intuitive. In particular, when one is concerned with obtaining insight into difficult problems, for example, the influence of microwave modulation on the atomic lineshape,[19] a two-level atom description is the most reasonable first step.

However, this approach is quantitatively incorrect and can even be in qualitative disagreement with reality under normal frequency standard operating conditions.[20] An alternative approach is to start from first principles and, as much as possible, to rigorously calculate collisional interactions, diffusion effects, and optical transmission profiles through the resonance cell.[21-24] This program will yield quantitatively correct results; however, in light of the number of interrelated physical processes that occur in the gas cell frequency standard, it appears to be an unreasonably complex procedure for predicting clock performance. Furthermore, as more physical processes are incorporated into the model, this rigorous approach will soon lose the intuitive nature that makes the two-level atom so attractive. Obviously, a middle approach is desirable, where important physical processes are recognized and treated fairly rigorously; whereas less important processes are treated by suitable simplifying approximations. In this regard, the starting point of the model to be presented subsequently is the generalized Vanier theory of the 0-0 hyperfine lineshape in optically pumped alkali-metal vapors.[6,20,25]

In the generalized Vanier theory, all the Zeeman sublevels of an alkali's ground state are considered. However, assume that: (1) all Zeeman sublevels of a given hyperfine multiplet interact with the light equivalently; (2) all Zeeman sublevels of the ground state have an equal probability of being populated as a result of decay from either the $5^2P_{3/2}$ or $5^2P_{1/2}$ excited states; and (3) the microwaves only induce transitions between the ($F = 2$, $m_F = 0$) and the (1,0) ground state Zeeman sublevels. Using these assumptions, the density matrix equations describing the evolution of the ground state Zeeman sublevels are considerably simplified. Additionally, relaxation of the ground state Zeeman sublevels is included phenomenologically into the model by considering "dark" longitudinal and transverse relaxation rates γ_1 and γ_2, respectively. Thus, one does not complicate the physical picture by differentiating among uniform, electron randomization and Zeeman relaxation mechanisms.[26] [At the present time, there appears to be no compelling reason for considering relaxation more rigorously (see Ref. 20).] In the remainder of this section, we will use the generalized Vanier theory to construct a

model for the transmitted light intensity as a function of microwave frequency in a gas cell frequency standard that is, possibly, optically thick. In this regard, our procedure for constructing the model will be to consider each important clock element and physical process individually before incorporating it into the evolving clock model.

1. LAMP AND FILTER CELL

We assume that the lamp light entering the resonance cell can be decomposed into five parts: four Gaussian lineshapes of full width $\Delta\nu_G$ corresponding to transitions 1-4 in Fig. 1b, and a component corresponding to the lamp's buffer gas light, which contributes to the shot noise at the photodetector. Defining ϵ as the ratio of total buffer gas light to total rubidium light, we have for the optical spectrum entering the resonance cell

$$I(\nu) = \sum_{i=1}^{4} I_{io}\left[\epsilon\delta(\nu - \nu_{BG}) + \frac{4\ln 2}{\pi\Delta\nu_G^2}\exp\left(-\frac{4\ln 2(\nu - \nu_i)^2}{\Delta\nu_G^2}\right)\right] \qquad (9)$$

where I_{io} is the total entrance intensity of line i, and ν_i is the center frequency of the i^{th} spectral component. The presence of the Dirac delta function $\delta(\nu - \nu_{BG})$ is a simple means of including lamp buffer gas light into the analysis. The I_{io} are determined by the properties of the lamp and the action of the filter cell, both of which have recently received considerable study.[27-31] Our model should be applicable to both the SFC and IFC Rb clock designs. This flexibility was included by allowing for an isotopic mixture in the resonance cell and by maintaining the I_{io} as input parameters to the model (so that the I_{io} can represent the direct spectral emission from either the lamp or the lamp/filter cell combination).

2. TRANSMITTED LIGHT

To take into account the effects of optical pumping on the light transmitted by the resonance cell, we write the Bouger-Lambert law for the spectral components as

$$\frac{\partial I_i(\Delta,z)}{\partial z} = -\eta_\Delta(z)[Rb^{87}]\sigma_i I_i(z) \quad (i = 1,2) \tag{10a}$$

$$\frac{\partial I_j(\Delta,z)}{\partial z} = -\left\{[1-\eta_\Delta(z)]\ [Rb^{87}] + \left(\frac{7}{12}\right)\ [Rb^{85}]\right\}\ \sigma_j I_j(z)\ (j = 3,4) \tag{10b}$$

Equation (10b) reflects the fact that spectral components 3 and 4 are absorbed by not only Rb^{87} atoms but also Rb^{85} atoms, which would be present if an IFC design were employed. In these expressions, $\eta_\Delta(z)$ is the fractional population in the F = 1 hyperfine multiplet at some axial position z in the resonance cell, and for some detuning Δ between the hyperfine transition frequency and the applied microwave field; $[Rb^{87}]$ and $[Rb^{85}]$ are number densities; and the σ_μ are optical absorption cross sections:

$$\sigma_\mu = 2r_o f_\mu c \sqrt{\pi \ell n 2/(\Delta\nu_G^2 + \Delta\nu_D^2)} \tag{11}$$

where f_μ is the μ^{th} transition oscillator strength, r_o is the classical electron radius, and $\Delta\nu_D$ is the Doppler broadened absorption linewidth. (Note that for an isotopically mixed resonance cell, we assume negligible optical pumping of the Rb^{85} isotope. Considering the low light levels involved, this is probably a reasonable first order approximation.)

We note that the present model of gas cell clock absorption is basically one dimensional; that is, in cylindrical coordinates we consider the transmitted intensity at a specific axial position z to be equivalent for all r and θ. In actuality, however, we know that this is not the case in presently manufactured designs, because the microwave field strength in the clock cavity can have both a radial and angular dependency.[32,33] Thus, as applied to presently available gas cell frequency standards, the present model must be considered as a first-order approximation. It is our belief, though, that corrections resulting from the radial and angular distribution of microwave field strength within the clock cavity are within the uncertainties generated

by the imperfect knowledge of the input parameters required by the model. Furthermore, it is likely that advanced gas cell frequency standards will employ dielectrically loaded cavities whose microwave fields have no radial or angular dependencies,[34] or photodetectors that only sample transmitted light intensities at specific values of r and θ.[32] For these advanced frequency standards, we expect our model to be somewhat more rigorous.

Integrating Eqs. (10a) and (10b), the intensity of the rubidium light at any axial position z is given by

$$I_i(\Delta,z) = I_{io} \exp\{-\overline{\eta_\Delta}(z)\,[Rb^{87}]\,\sigma_i z\} \quad (i = 1,2) \tag{12a}$$

$$I_j(\Delta,z) = I_{jo} \exp\left(-\left\{[1 - \overline{\eta_\Delta}(z)]\,[Rb^{87}] + \left(\frac{7}{12}\right)[Rb^{85}]\right\}\sigma_j z\right) \quad (j = 3,4) \tag{12b}$$

where $\overline{\eta_\Delta}(z)$ is the fractional population in the F = 1 hyperfine multiplet averaged over the vapor length traversed by the light:

$$\overline{\eta_\Delta}(z) \equiv \left(\frac{1}{z}\right) \int_0^z \eta_\Delta(z)\, dz \tag{13}$$

[For convenience, at $z = \ell$, $\overline{\eta_\Delta}(\ell)$ will simply be denoted as $\overline{\eta_\Delta}$.] Thus, the quantity of interest for determining clock performance becomes

$$I(\Delta,\ell) = \sum_{i=1}^{2} I_{io}\left(\varepsilon + \exp\{-\overline{\eta}_\Delta[Rb^{87}]\,\sigma_i\ell\}\right)$$

$$+ \sum_{j=3}^{4} I_{jo}\left| \varepsilon + \exp\left(-\{(1 - \overline{\eta}_\Delta)\,[Rb^{87}] + \left(\frac{7}{12}\right)[Rb^{85}]\}\sigma_j\ell\right)\right|. \tag{14}$$

This equation is deceptively simple in appearance. The transmitted light

intensity is just the sum of several exponential functions. In actuality, the $\overline{\eta}_\Delta$ terms appearing in the exponents greatly complicate the situation, because they depend on the $I_i(z)$. Thus, the equation for $I(\Delta,\ell)$ is transcendental and requires special consideration. Note that the transcendental nature of Eq. (14) results solely from the fact that under normal clock operating conditions, the resonance cell's alkali vapor is optically thick to the rubidium lamp light. For an optically thin vapor, $\overline{\eta}_\Delta$ would be a function of the given $I_{\mu o}$.

3. THE FRACTIONAL POPULATION η_Δ

In the generalized Vanier theory, the fractional population in the lower F = b = I - 1/2 hyperfine multiplet, where I is the alkali's nuclear spin and diffusion is considered phenomenologically, is given by the expression[20]

$$\eta'_\Delta = \left[\frac{g_b(A + \gamma_1)}{g_a(B + \gamma_1) + g_a(A + \gamma_1)}\right] \left[\frac{\Gamma_2^2 + \Delta^2 + (\Gamma_2/\Gamma_{1\alpha})\,\omega_1^2}{\Gamma_2^2 + \Delta^2 + (\Gamma_2/\Gamma_{1\beta})\,\omega_1^2}\right] \tag{15}$$

where

$$\Gamma_2 = \frac{(A + B)}{2} + \gamma_2 \tag{16}$$

$$\Gamma_{1\alpha} = (B + \gamma_1)\left[1 + \left(\frac{g}{4g_b}\right)\left(\frac{B - A}{A + \gamma_1}\right)\right]^{-1} \tag{17}$$

and

$$\Gamma_{1\beta} = \frac{(A + \gamma_1)(B + \gamma_1)(g_a B + g_b A + g\gamma_1)}{g[(A + B)/2]^2 + A(B - A) + \gamma_1\{g[(A + B)/2 + \gamma_1] + g_a B + g_b A\}} \tag{18}$$

In these expressions, the subscripts a and b refer to the F quantum numbers of the hyperfine multiplets (e.g., a = I + 1/2), and ω_1 is the microwave Rabi frequency. The g's refer to the various degeneracies in the alkali ground

state: g is the total ground state degeneracy equal to $2(2I + 1)$, g_a is the degeneracy of the upper F = a hyperfine multiplet equal to $2(I + 1)$, and g_b is the degeneracy of the lower hyperfine multiplet equal to 2I (for Rb^{87} g = 8, g_a = 5, and g_b = 3). The terms A and B are defined as optical photon absorption rates for the F = 2 and F = 1 hyperfine multiplets, respectively. Because of the variation of optical pumping light intensity with axial position, the magnitudes of these quantities depend on z. The calculation of A and B is carried out subsequently. The quantities which depend on axial position A, B, and ω_1 result in η_Δ' also displaying an axial dependence. However, because of the inclusion of the effects of atomic axial diffusion, the quantity of interest η_Δ has a different axial dependence than η_Δ', though, as shown below, there is a relatively simple expression relating them.

Probably the stickiest issue for the generalized Vanier theory to handle is that of atomic diffusion. In uncoated resonance cells, after an alkali atom hits the wall, the population density distribution among all of the atom's ground state Zeeman sublevels is randomized.[35] Thus, the measure of hyperfine polarization $\langle \hat{I} \cdot \hat{S} \rangle$ is zero at the resonance cell walls. Rigorously, a term $D\nabla^2\rho$ must be included into the density matrix rate equations in order to describe diffusion, where D is the diffusion coefficient of Rb atoms in the resonance cell's vapor.[36] However, in the generalized Vanier theory, diffusion is considered as a phenomenological relaxation mechanism, contributing a term γ_{dif} to both γ_1 and γ_2. If R is taken as a measure of the resonance cell's dimensions, typically, the resonance cell's radius, then $\gamma_{dif} = D/R^2$. This procedure for including diffusion into the determination of η_Δ is actually quite reasonable, because if no other relaxation mechanisms were present, η_Δ would relax in the dark (i.e., in the absence of optical pumping light and microwaves) with a rate of this order of magnitude.[37] However, diffusion is fundamentally different from other "bulk" relaxation mechanisms like Rb-buffer gas and Rb-Rb collisions, because, in steady state, diffusion leads to a spatial distribution of $\langle \hat{I} \cdot \hat{S} \rangle$. The bulk relaxation mechanisms only affect the magnitude of $\langle \hat{I} \cdot \hat{S} \rangle$, not its spatial distribution.

Minguzzi et al.[38] have shown that the spatial distribution of $\langle \hat{I} \cdot \hat{S} \rangle$ is, in general, characterized by a sum of diffusion modes. In the case of the gas

cell clock, though, where the optical pumping rate is low and the resonance cell is fairly uniformly illuminated, a reasonable approximation is to consider only the first order mode. Thus, we have for the axial distribution of $\langle \hat{I} \cdot \hat{S} \rangle$

$$\langle \hat{I} \cdot \hat{S} \rangle (z) \approx \langle \hat{I} \cdot \hat{S} \rangle_p \sin (\pi z/\ell) \tag{19}$$

Because η_Δ is simply related to $\langle \hat{I} \cdot \hat{S} \rangle$ by the equation[39]

$$\eta_\Delta = \frac{1}{2} - \frac{4\langle \hat{I} \cdot \hat{S} \rangle + 1}{g} \tag{20}$$

we have for the spatial distribution of η_Δ, considering only the first order axial diffusion mode,

$$\eta_\Delta(z) = \frac{g_b}{g} + (\eta'_\Delta - \frac{g_b}{g}) \sin (\frac{\pi z}{\ell}) \tag{21}$$

In essence, we have decomposed the contributions of diffusion to η_Δ into two parts. In the first part, we assume that diffusion has some limiting effect on the magnitude of η_Δ, and that this effect can be incorporated into the generalized Vanier theory through contributions to γ_1 and γ_2. In the second part, we recognize that the final form of the axial distribution of η_Δ is to some degree known, so a functional form can be superimposed onto the solution η'_Δ. In this way, the major physical aspects of diffusion are brought into the model without recourse to cumbersome and obscure expressions.

The bulk relaxation mechanisms which contribute to γ_1 and γ_2 are typically buffer gas and spin exchange collisions. Additionally, for completeness, one should incorporate the slowdown factor, $(6I + 1)/(8I + 4)$, into the spin exchange contribution to the transverse relaxation rate γ_2.[25] Thus, if we define σ_{BG} and σ_{ex} as the buffer gas relaxation and spin exchange cross

sections, respectively,[40,41] the phenomenological relaxation rates γ_1 and γ_2 become

$$\gamma_1 = D/R^2 + [BG]\,\bar{v}\sigma_{BG} + [Rb]\bar{v}\sigma_{ex} \tag{22a}$$

and

$$\gamma_2 = D/R^2 + [BG]\bar{v}\sigma_{BG} + \left(\frac{6I + 1}{8I + 4}\right)[Rb]\bar{v}\sigma_{ex} \tag{22b}$$

where [BG] is the number density of buffer gas molecules or atoms, and $\bar{v}$ is the average relative velocity between colliding species.

Finally, by assuming that the Rb atoms are essentially frozen in place because of the presence of the buffer gas,[33,42,43] we can determine $\eta'_\Delta(z)$ by substitution of the position dependent photon absorption rates, A and B, along with the suitable expression describing $\omega_1(z)$ into Eq. (15). For typical gas cell frequency standards employing a TE_{011} or TE_{111} microwave cavity this expression is simply[44]

$$\omega_1(z) = \omega_{1p} \sin\left(\frac{\pi z}{\ell}\right) \tag{23}$$

where ω_{1p} is the peak microwave Rabi frequency in the cavity.

4. DETERMINATION OF THE DEPENDENCE OF PHOTON ABSORPTION RATES ON AXIAL POSITION

To calculate the positional dependencies of the optical photon absorption rates, we first assume that the axial optical intensity distribution can be approximated by a Bouger-Lambert law of the form

$$I_i(\zeta,z) = I_{io} \exp\{-\zeta[Rb^{87}]\,\sigma_i z\} \qquad (i = 1, 2) \tag{24a}$$

$$I_j(\zeta,z) = I_{jo} \exp\left(-\{(1-\zeta)[Rb^{87}] + (\tfrac{7}{12})\,[Rb^{85}]\}\sigma_j z\right) \qquad (j = 3, 4) \tag{24b}$$

where ζ is to be thought of as a resonance cell parameter describing the "global" fractional population in the F = 1 hyperfine multiplet as a result of optical pumping. In effect, ζ is a zeroth order approximation to $\eta'_\Delta(z)$. For the low optical pumping rates expected from lamps, this approximation should be a reasonable description of reality, because in the limit of negligible optical pumping, $\bar{\eta}_\Delta(z)$ in Eqs. (12a) and (12b) is independent of the light intensity, and the standard Bouger-Lambert law is recovered. We note, however, that recent theoretical work has indicated that this approximation may not be generally valid.[22,23] Equations (24a) and (24b) will permit us to calculate the positionally dependent optical photon absorption rates as functions of ζ:

$$A(\zeta, z) = (\tfrac{1}{h\nu}) \sum_{j=3}^{4} I_j(\zeta, z)\sigma_j \tag{25a}$$

$$B(\zeta, z) = (\tfrac{1}{h\nu}) \sum_{i=1}^{2} I_i(\zeta, z)\sigma_i \tag{25b}$$

The task which now needs to be discussed is the determination of ζ. Considering Eqs. (14) and (24), it is clear that any consistent choice of ζ must satisfy the equation

$$\sum_{k=1}^{4} I_k(\zeta,\ell) = \sum_{i=1}^{2} I_{io} \exp\{-\bar{\eta}_\infty\,[Rb^{87}]\sigma_i\ell\}$$

$$+ \sum_{j=3}^{4} I_{jo} \exp\left(-\{(1 - \bar{\eta}_\infty)[Rb^{87}] + (\tfrac{7}{12})\,[Rb^{85}]\}\sigma_j \ell\right) \qquad (26)$$

The simplest choice of ζ which satisfies this requirement is

$$\zeta = \bar{\eta}_\infty = \frac{1}{\ell} \int_0^\ell \eta_\infty \, dz \qquad (27)$$

Substituting Eqs. (15) and (21) into Eq. (27), our expression for ζ becomes

$$\zeta - \frac{g_b}{g} + \frac{g_b g_a}{\ell g} \int_0^\ell \left\{ \frac{[B(\zeta) - A(\zeta)] \sin(\frac{\pi z}{\ell})}{g_a[B(\zeta) + \gamma_1] + g_b[A(\zeta) + \gamma_1]} \right\} dz = 0 \qquad (28)$$

where we have explicitly noted that A and B depend parametrically on ζ. Using a Newton-Raphson method,[45] we can solve Eq. (28) numerically for ζ. A discussion of the results of this procedure for determining ζ and their consistency will be presented subsequently.

In summary, with the determination of ζ, A(z) and B(z) are specified and when substituted into Eq. (15), determine η'_Δ. The terms η_Δ and $\bar{\eta}_\Delta$ follow directly from η'_Δ via Eqs. (21) and (13), respectively. Substituting $\bar{\eta}_\Delta$ into Eq. (14) yields the transmitted light intensity $I(\Delta, \ell)$ and the optically detected hyperfine lineshape, $S(\Delta) = I(\infty, \ell) - I(\Delta, \ell)$.

C. INTEGRATION OF ATOMIC PHYSICS WITH FEEDBACK ANALYSIS

It is a straightforward process to extract the quantities required by the feedback analysis from the preceding study of the physics occurring in the absorption cell. If κ and A_p are the clock photodiode's sensitivity (A/W) and area, which is assumed to be identical to the clock cavity's cross-sectional area, the total lamp induced photocurrent is given by

$$i_o = \kappa A \, I(\infty, \ell) \qquad (29)$$

The slope of the discrimination pattern is given by

$$m = \delta_m \, I''(0, \ell) \tag{30}$$

where $2\delta_m$ is the modulation depth of the microwave frequency, and $I''(0, \ell)$ is the second derivative of the transmitted light intensity evaluated at the center frequency of the hyperfine resonance. By equating the slope of the discriminator pattern with $\delta_m \, I''(0, \ell)$, we have made the small-modulation-depth/quasi-static approximation with regards to the effect of the microwave frequency modulation on the signal lineshape.[7] As long as we confine ourselves to frequency modulation regimes such that $\delta_m/\Gamma_2 \sim 1$ and $\omega_M/\Gamma_2 \sim 1$, where ω_M is the modulation frequency, then the recent work of Audoin et al.[19] would indicate that this approximation is reasonably valid. As will be demonstrated in the following paragraphs, the exclusion of higher order modulation effects does not appear to have affected the ability of our model to accurately predict the performance of current generation Rb clocks. It is not clear, though, that this would be true under all potential clock operating conditions. If clock conditions varied significantly from nominal values used in current standards, the ramifications of microwave modulation would have to be reconsidered. However, these effects could be approximated in the present model by using the work of Audoin et al.[19] to determine a correction factor for Eq. (30). In our calculations, δ_m is considered equal to the frequency separation of the inflection points of the approximately Lorentzian resonance lineshape, and it is assumed that $\omega_M < \delta_m$.

III. MODEL VERIFICATION

In the model of the clock signal lineshape just presented, quite a few assumptions were made in order to make the problem tractable. Several of these assumptions are inherent to the generalized Vanier theory and have been validated by recent experimentation.[20] These can be considered as microscopic assumptions, because they are related to the statistical behavior of individual atoms. The other assumptions in the model (i.e., the functional form of the axial light intensity distribution, and the axial distribution of η_Δ as a result of diffusion) should be considered as macroscopic assumptions, because they are related to the alkali vapor as a whole. We are on less firm ground experimentally with these assumptions. Thus, before proceeding to calculations of clock performance, it would be prudent to explore the validity of these assumptions. This will be accomplished by showing that the model, in its present form, leads to qualitatively correct predictions of the global fractional population ζ, the axial distribution of $\langle \vec{I} \cdot \vec{S} \rangle$, and the signal lineshape as functions of temperature.

The global fractional population ζ is actually a quite useful parameter for understanding gas cell clock performance, because it reflects the degree of optical pumping, and hence the clock signal amplitude, for the resonance cell as a whole. Qualitatively, one expects ζ to depend on temperature in two ways: (1) as the resonance cell temperature rises, the global optical pumping rate necessarily changes; and (2) the longitudinal relaxation rate is temperature dependent as a result of spin exchange. Thus, for high temperatures, one expects ζ to approach its statistical value g_b/g. At low temperatures, when the vapor is optically thin, one should be able to arrive at a relatively simple expression for ζ because in this case, one can assume that A and B are constants independent of axial position. Regarding Eq. (28) in this optically thin regime, one has

$$\zeta_{thin} = \frac{g_b}{g} \left\{ 1 - \frac{2g_a(B - A)}{\pi[g_a(B + \gamma_1) + g_b(A + \gamma_1)]} \right\} \tag{31}$$

which is still a temperature dependent quantity because of γ_1.

If we now consider the case of optical pumping out of only the F = b hyperfine multiplet, as a specific example, the preceding arguments would require us to make the following predictions regarding ζ: (1) at low resonance cell temperatures, ζ should be relatively small; (2) at high temperatures, ζ should saturate at 3/8 in the case of Rb; and (3) for intermediate temperatures one should have $\zeta_{correct} > \zeta_{thin}$, because ζ_{thin} increases as a function of temperature as a result of only one mechanism, whereas $\zeta_{correct}$ increases as a result of two cooperating mechanisms. A sample calculation of ζ over the temperature range 10-120°C is presented in Fig. 3. The qualitative agreement between our expectations and the calculations lends confidence to the interpretation and use of ζ in the clock signal model.

Because the atoms are essentially frozen in place as a result of the presence of the buffer gas, the maximum change in light intensity per unit length (for microwaves on and off resonance) occurs in a unique spatial region of the resonance cell determined by the light intensity distribution, the microwave field distribution, and diffusion. The ability to determine this unique spatial region is critically important for a model of gas cell clock performance, because the microwave field strength and light intensity in this region have the primary influence on both the clock's Q and signal-to-noise ratio. Furthermore, variations in this position with microwave power and light intensity are responsible for the so-called position shift[42] and inhomogeneous light shift,[43] respectively.

As previously discussed, the present model is one dimensional. Thus, if the model is to be trusted in clock performance predictions, it should be able to predict the qualitatively correct axial distribution of $\langle \hat{I} \cdot \hat{S} \rangle$ as a function of resonance cell temperature. For the case of an optically thin cell and relatively low optical pumping light intensities, one would expect a distribution of $\langle \hat{I} \cdot \hat{S} \rangle$ peaked in the center of the resonance cell. As the resonance cell temperature was raised, and as the cell became more opaque to the optical pumping light, one would expect the position corresponding to the maximum $\langle \hat{I} \cdot \hat{S} \rangle$ to shift towards the front of the resonance cell. In Fig. 4, we have plotted the model's predictions of $\langle \hat{I} \cdot \hat{S} \rangle$ as a function of axial position using the parameters listed in Table 1. We note that the curves are

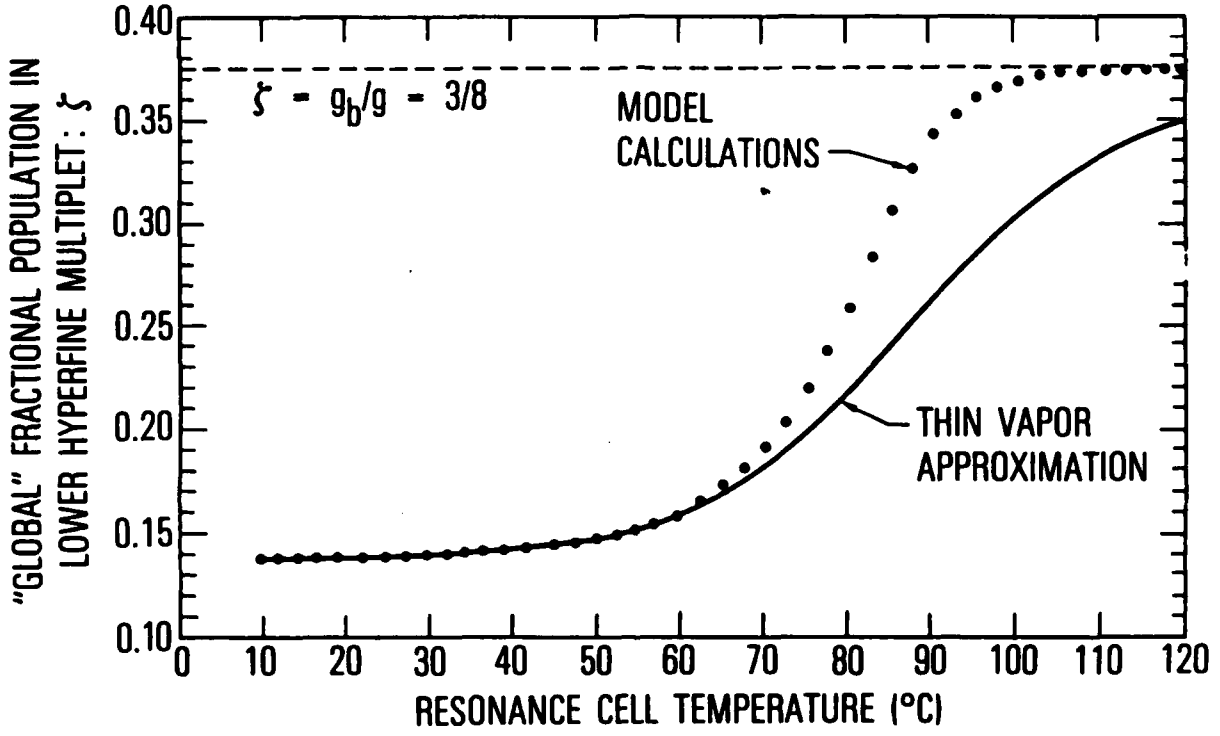

Fig. 3. Global Fractional Population ζ in the F = b = I - 1/2 Hyperfine Multiplet as a Function of Resonance Cell Temperature for the Case of Optical Pumping Out of Only This Multiplet. The solid line is a thin vapor approximation where the spin exchange rate is the only temperature dependent quantity; dots correspond to the actual case where the optical thickness of the vapor must also be considered. In the limit of no optical pumping, the equilibrium value of ζ is 3/8.

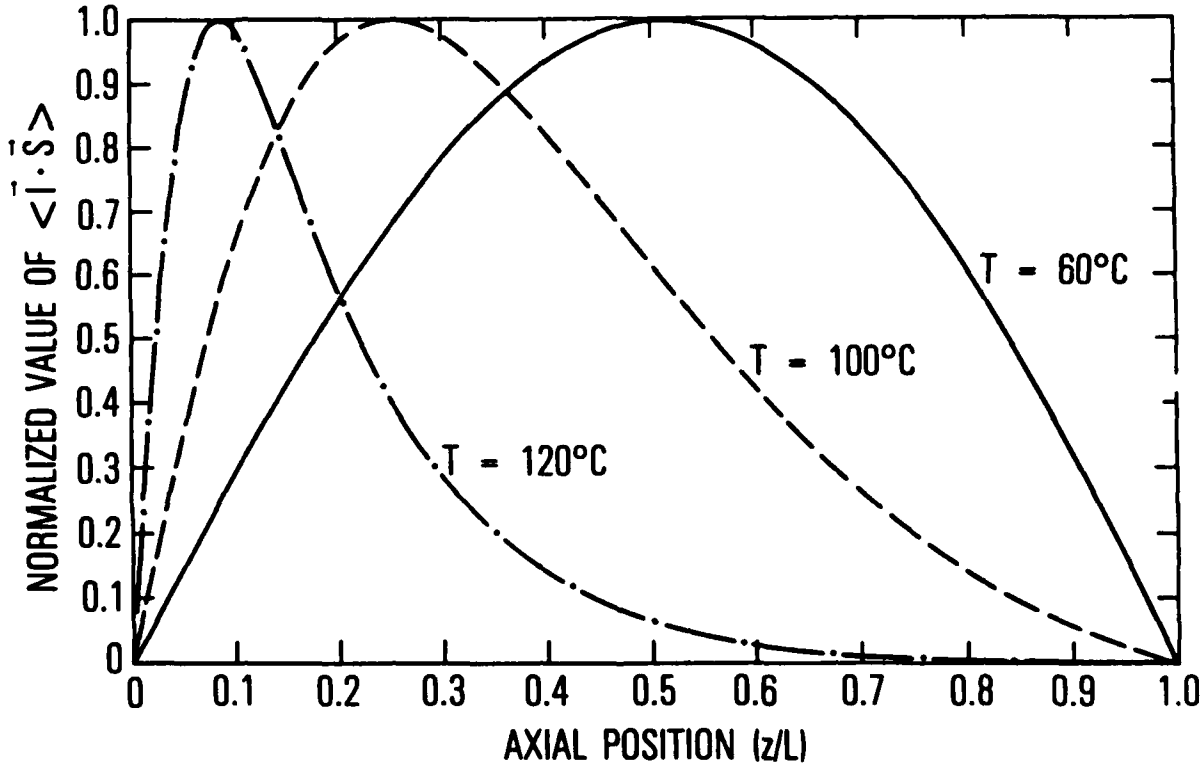

Fig. 4. The Measure of Hyperfine Polarization $\langle \hat{I} \cdot \hat{S} \rangle$ has an Axial Spatial Distribution That is Temperature Dependent. For relatively low resonance cell temperatures, the spatial distribution is primarily determined by diffusion. As the resonance cell's alkali-metal vapor becomes progressively more optically thick, efficient optical pumping becomes confined to regions closer to the entrance window of the resonance cell.

Table 1. Parameters for Clock Signal Model

Parameter	Value[a]	Uncertainty
Linewidth of lamp lines	2 GHz	± 0.2 GHz
Temperature	65°C	± 5°C
Photodiode responsivity	0.5 A/W	
Ratio of buffer gas light to Rb resonance light	0.64	
$P_o(D_1, F = 1)$	0.029 mW	± 5%
$P_o(D_2, F = 1)$	0.046 mW	
$P_o(D_1, F = 2)$	0.018 mW	∓5% (b)
$P_o(D_2, F = 2)$	0.029 mW	
Peak Rabi frequency ω_{1p}	450 Hz	
Buffer gas	N_2	
Buffer gas pressure	10 Torr	
Light shift coefficient	-3×10^{-10} (c)	$\pm 1 \times 10^{-10}$
Lamp intensity spectral density	$1.2 \times 10^{-9} + \frac{1.3 \times 10^{-13}}{f^2}$ (c)	

[a] Ref. 9

(b) Optical powers were varied in the calculations according to the rule that if $P_o(D_i, F = 1)$ changed by ± 5%, then simultaneously $P_o(D_i, F = 2)$ changed by ∓ 5%.

[c] Ref. 16

very similar to those of Minguzzi et al.,[38] where the effects of diffusion were analyzed more rigorously, and are again in qualitative agreement with our expectations.

Of course, the most critical test for our macroscopic assumptions concerns the signal lineshape. Experimentally, it is known that the transmission signal resonance is very well approximated by a Lorentzian, being, however, somewhat more sharply peaked.[46] Regarding the model, there is no reason a priori to expect a lineshape resembling anything like a Lorentzian; yet if this is not predicted over a reasonable range of operating temperatures, the validity of the model must be questioned. In Figs. 5a and 5b, we show the signal lineshape calculated at 20 and 100°C, respectively, using the parameters listed in Table 1. The dots are model calculations, and the solid curve is a least squares fit of the model results to a Lorentzian. As is readily apparent, the model gives excellent agreement in the wings of the lineshape, but near resonance is more sharply peaked, as expected. These predictions are in qualitative agreement with the experimental results of Camparo and Frueholz.[46] Thus, our macroscopic assumptions appear to be valid, at least over normal clock operating conditions, permitting the final test of the model: a comparison between predicted and measured Rb gas cell clock performance.

Recently, Riley[9] and Lynch and Riley[10] performed a stability test on a newly designed Rb frequency standard. This test was somewhat unique, because many of the input parameters required by the present model of clock performance were documented. Thus, these results can be used to establish the accuracy of the present model in predicting clock performance. The parameters required for the calculation are listed in Table 1, along with reasonable estimates of their values, based on the information presented by Riley or on our own measurements on similar components of the Rb clock. The uncertainties presented with some of the more critical parameters represent our best estimates of the inaccuracies associated with extracting the parameters from the information presented by Riley. In particular, the uncertainty associated with the resonance cell temperature represents the difficulty associated with measuring liquid alkali metal temperatures accurately, and the difficulty of

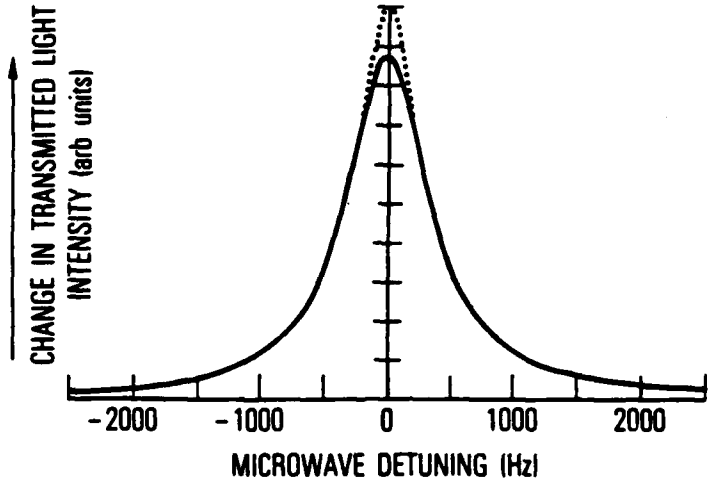

(a)

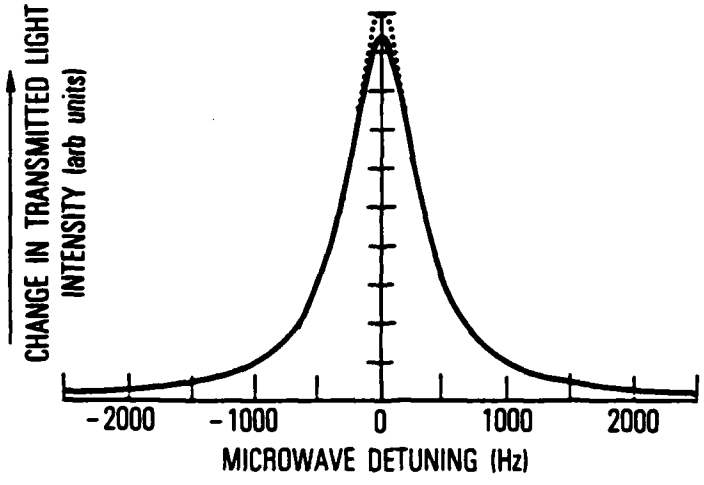

(b)

Fig. 5. Optically Detected Hyperfine Transition Lineshape. (a) T = 20°C, (b) T = 100°C. The dots are the calculated change in transmitted light intensity as a function of microwave frequency; the solid curve is a least squares Lorentzian fit. Note that at reasonable resonance cell temperatures, the lineshapes are well approximated by a Lorentzian; they are, however, somewhat more sharply peaked.

accurately converting these liquid temperatures to saturated alkali vapor pressures. The only parameter that could not be determined by the information presented by Riley was the peak Rabi frequency. This parameter was, therefore, evaluated by matching the calculated signal linewidth with Riley's measured signal linewidth. We note, however, that this parameter can be determined experimentally quite easily by the adiabatic rapid passage method of Frueholz and Camparo.[33] The choice of buffer gas was not crucial, so, for convenience, nitrogen at 10 Torr was used.

Table 2 and Fig. 6 display the results of our calculations along with uncertainties in the calculated quantities which are associated with the uncertainties in the input parameters. Several points concerning the predicted results are worth noting. First, the predicted Q and discriminator slope agree very well with the measured values, especially because the measured discriminator slope is probably a bit too large. Based on the measured Allan variance and DC photocurrent, one would have expected to measure a discriminator slope of 268 pA/Hz. Furthermore, the results indicate that the line Q is relatively insensitive to reasonable variations in the global optical pumping rate, but that the signal amplitude is very sensitive to these changes. This is precisely the same conclusion reached by Matsuda et al. in their experimental studies of the signal characteristics of the Rb gas cell clock.[47] Finally, the calculated Allan variance agrees very well with that measured by Lynch and Riley,[10] as shown by Fig. 5. Thus, within the uncertainties associated with the input parameters, we have demonstrated the validity of a model of gas cell clock performance that is completely independent of measurements of the clock signal's Q or signal-to-noise ratio.

Vanier et al. have carried out extensive analyses of the effect of loop attack time on clock performance. As an additional demonstration of the model capabilities, the Allan variances for two different servo-control loop attack times are calculated. The crystal oscillator is assumed to have a power spectral density of fractional frequency fluctuations of[17]

$$S_y^{cr}(f) = \frac{6 \times 10^{-26}}{f} + 1 \times 10^{-26} f + 2 \times 10^{-28} f^2 \qquad (32)$$

Table 2. Comparison of Predicted Clock Performance with Measured Clock Performance

Quantity	Predicted Valve	Measured Valve
Fractional Population ζ	0.359	
Fraction Population Change: $\eta_o - \zeta$	4.3×10^{-3}	
DC photocurrent	81.8 μA	82 μA
Photocurrent change: $i_{dc} - i_{\Delta=0}$	$(45.7^{+35\%}_{-30\%})$ nA	
Q:	$(1.63^{+1.2\%}_{-1.8\%}) \times 10^7$	1.6×10^7
Discriminator pattern slope: $\delta_m I''(0,\ell)$	(251^{+93}_{-74}) pA/Hz	351 pA/Hz
Short-Term Allan variance: $\sigma_y(\tau)$	$(3.1^{+1.1}_{-0.9}) \times 10^{-12}/\sqrt{\tau}$	$2.8 \times 10^{-12}/\sqrt{\tau}$

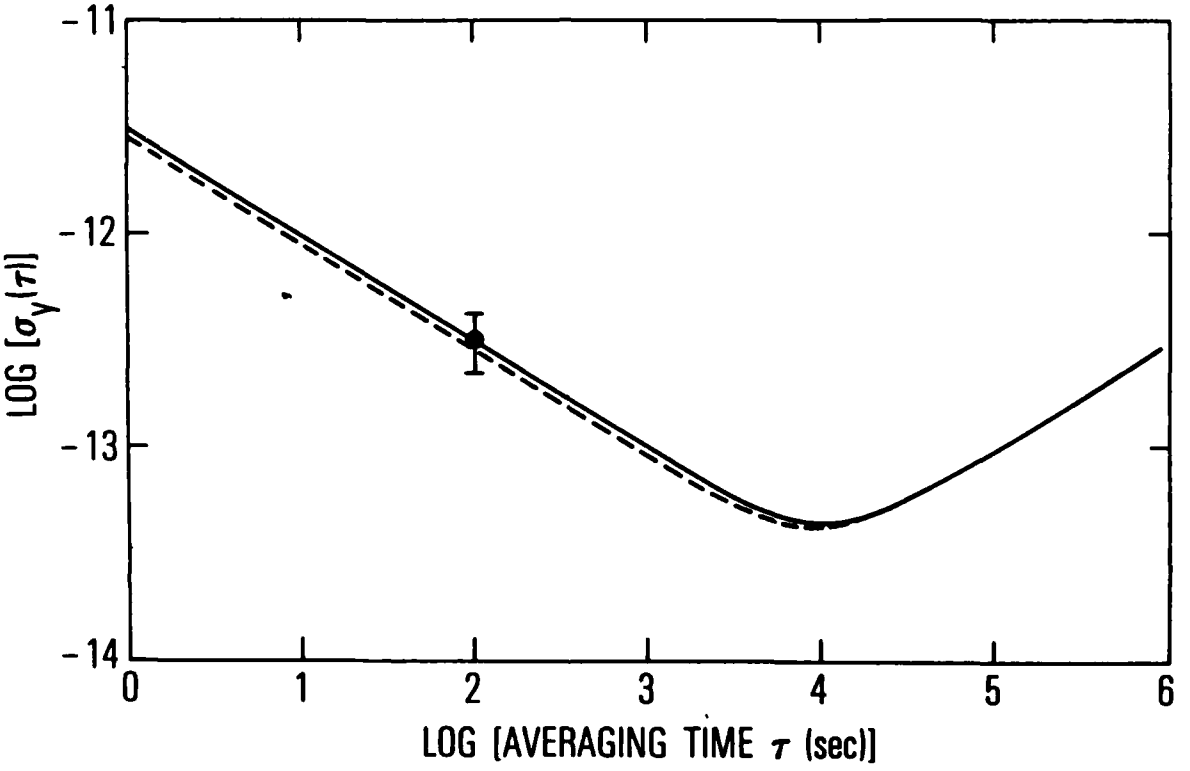

Fig. 6. Frequency Stability of the EG&G Rb Gas Cell Frequency Standard in Terms of Allan Variance $\sigma_y(\tau)$. The dashed line is the standard's experimental performance, while the solid line is the predicted performance yielded by the model. The error bar represents the uncertainty in the standard's predicted performance due to uncertainties in the input parameters. For averaging times less than 10^4sec, the standard's performance is limited by shot noise at the photodetector. When the averaging time is greater than 10^4sec, clock performance is limited by discharge lamp intensity fluctuations transferred into frequency fluctuations through the light shift effect.

while the atomic system behaves as previously calculated. Two attack times, 0.1 and 10 sec, are considered. The resultant Allan variances are displayed in Fig. 7. These results were calculated quite efficiently because of the analytical evaluation of the integrals of Eq. (8). As an aside, we note that the present analysis of the hyperfine lineshape, based on the quasi-static approximation, will not be valid at extremely short attack times. At very short attack times the Rb atoms will no longer be able to respond adiabatically to the microwave frequency variation induced by the control loop. Furthermore, at short attack times, atomic coherence effects should be considered. For typical gas cell frequency standards, a reasonable limit to the validity of our model would be an attack time of 0.01 sec.

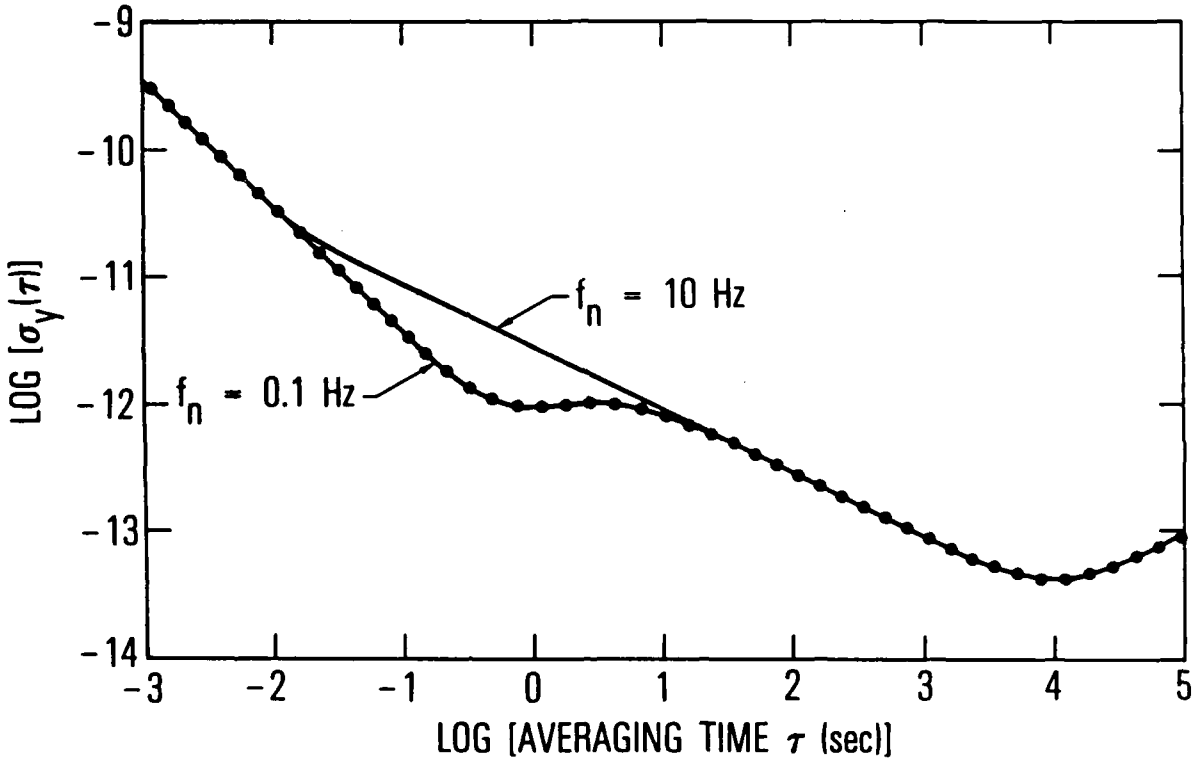

Fig. 7. Calculated Allan Variance $\sigma_y(\tau)$ for Passive Rb^{87} Gas Cell Standard for Two Control Loop Attack Times. Crystal oscillator performance as specified in Ref. 17. The atomic system performance is that of the EG&G prototype standard.

IV. CONCLUSIONS AND SUMMARY

In practice, a clock model's usefulness is intimately connected to the realization of a device with optimal performance characteristics for a specific application. Thus, though reasonable accuracy in model predictions is required, equally important attributes of a clock model are its ability to: (1) analyze design trade-offs for a specific application, (2) diagnose the clock parameters that limit performance, and (3) predict the avenues for further improvement. Because the present model is inherently numerically faster than its predecessors, as a result of the analytic evaluation of the spectral density integrals and density matrix inversion, design trade-offs can be quickly evaluated. Furthermore, because the model treats the physics of the resonance cell signal in a semirigorous yet perspicuous manner, diagnoses of performance limits and predictions for improvements are in terms of physically meaningful and conceptually lucid parameters.

As an example of the present model's ability to predict possible avenues of improvement for the Rb gas cell clock, we have computed the short-term performance for a clock with the parameters listed in Table 1 as a function of microwave power, or what is equivalent to the peak Rabi frequency in the clock cavity. These results are shown in Fig. 8. As is clear from the figure, the model predicts that a short-term stability of $6 \times 10^{-13}/\sqrt{\tau}$ could be achieved by reducing the 6835 MHz microwave power fed into the cavity by 23 dB. Of course, these predictions must be tempered by the realization that, for these Rabi frequencies, one might not be in the small-modulation-depth/quasi-state regime with regard to the discriminator slope, and that the microwave field strength displays only a longitudinal variation within the absorption cell. However, the predictions do indicate a possible avenue for improvement that must be experimentally verified.

Finally, with a straightforward modification, the microwave detuning in Eq. (9) can be made to depend upon local magnetic field strengths, local optical pumping light intensities, the buffer gas pressure, the alkali vapor pressure, etc. The model lineshape would then exhibit the inhomogeneous

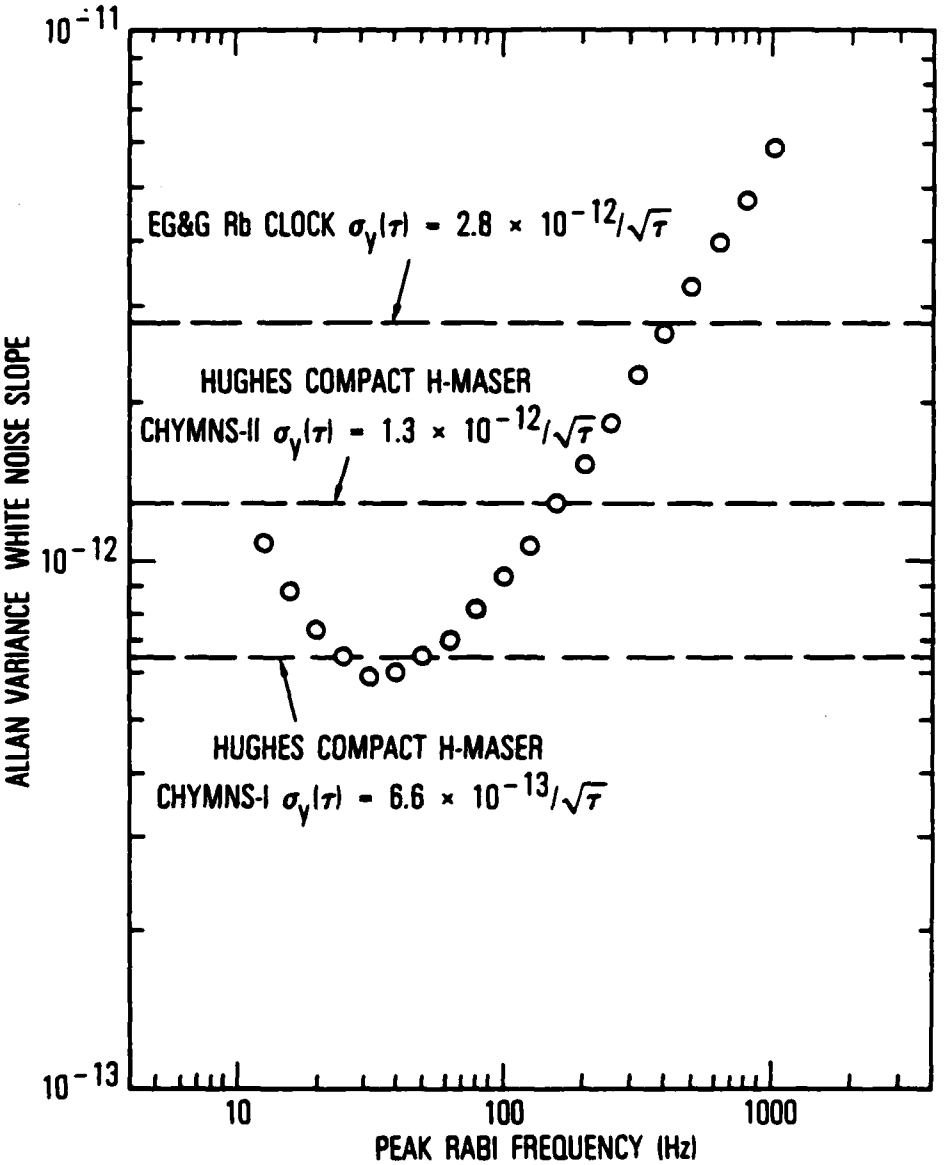

Fig. 8. Short-Term Allan Variance Slope for the Parameters of Table 1 as a Function of Microwave Rabi Frequency, or Equivalently, Microwave Power Fed into the Cavity Assuming a Q = 100. These calculations would indicate roughly a factor of 5 improvement in the short-term performance by decreasing the microwave power by ~ 23 dB.

nature that results in the position shift effect[42] and the inhomogeneous light shift.[43] With the inclusion of these resonant frequency shift terms, the model could be used to investigate possible mechanisms of gas cell clock frequency drift, which is a principal impediment to the gas cell frequency standard's more widespread use.

REFERENCES

1. J. M. Andres, D. J. Farmer, and G. T. Inouye, IRE Trans. Mil. Elec. MIL-3, 178 (1959); R. J. Carpenter, E. C. Beaty, P. L. Bender, S. Saito, and R. O. Stone, IRE Trans. Instrum. I-9, 132 (1960); M. E. Packard and B. E. Swartz, IRE Trans. Instrum. I-11, 215 (1962).

2. E. Jechart, Proceedings of the Twenty-Seventh Annual Symposium on Frequency Control, USAEC, Fort Monmouth, NJ (1973), p. 387.

3. J.-P. Gourber, Ann. Radioele. 20, 191 (1965).

4. R. F. Lacey, A. L. Helgesson, and J. H. Holloway, Proc. of IEEE 54, 170 (1966).

5. H. Fukuyo, K. Iga, N. Kuramochi, I. Matsuda, and H. Ishikawa, Bull. Tokyo Inst. Tech. 107, 75 (1971).

6. G. Missout and J. Vanier, Can. J. Phys. 53, 1030 (1975).

7. J. Vanier and L.-G. Bernier, IEEE Trans. Instrum. Meas. IM-30, 277 (1981).

8. J. C. Camparo, "The Diode Laser in Atomic Physics," Contemporary Physics (to be published).

9. W. J. Riley, Proceedings of the Thirteenth Annual Precise Time and Time Interval (PTTI) Application and Planning Meeting, NASA Conference Publication 2220, NASA, Greenbelt, MD (1981), p. 609.

10. T. J. Lynch and W. J. Riley, Proceedings of the Fifteenth Annual Precise Time and Time Interval (PTTI) Applications and Planning Meeting, Naval Research Laboratory, Washington, DC (1984), p. 269.

11. J. A. Barnes, A. R. Chi, L. S. Cutler, D. J. Healey, D. B. Leeson, T. E. McGunigal, J. A. Mullen, Jr., W. L. Smith, R. L. Sydnor, R. F. C. Vessot, and G. M. R. Winkler, IEEE Instrum. Meas. IM-20, 105 (1971).

12. L. S. Cutler and C. L. Searle, Proc. IEEE 54, 136 (1966).

13. J. Vanier, M. Tetu, and L. G. Bernier, IEEE Trans. Instrum. Meas. IM-28, 188 (1979).

14. A. Kastler, J. Opt. Soc. Am. 53, 902 (1963).

15. B. S. Mathur, H. Tang, and W. Happer, Phys. Rev. 171, 11 (1968).

16. C. H. Volk and R. P. Frueholz, J. Appl. Phys. 57, 980 (1985).

17. C. Audoin and J. Vanier, J. Phys. E. Sci. Instrum. 9, 697 (1976).

18. W. E. Bell and A. L. Bloom, Phys. Rev. 107, 1559 (1957).

19. C. Audoin, J. Viennet, N. Cyr, and J. Vanier, Proceedings of the Fourteenth Annual Precise Time and Time Interval (PTTI) Applications and Planning Meeting, NASA Conference Publication 2265, NASA, Greenbelt, MD (1983), p. 87.

20. J. C. Camparo and R. P. Frueholz, Phys. Rev. A 31, 1440 (1985).

21. V. V. Batygin, M. B. Gornyi, and B. G. Matisov, Sov. Phys. Tech. Phys. 26, 1314 (1982).

22. M. B. Gornyi, D. L. Markman, and B. G. Matisov, Opt. Spectrosc. 55, 20 (1983).

23. M. B. Gornyi and B. G. Matisov, Opt. Spectrosc. 56, 380 (1984).

24. M. B. Gornyi and B. G. Matisov, Sov. Phys. Tech. Phys. 28, 25 (1983).

25. J. Vanier, Phys. Rev. 168, 129 (1968).

26. F. A. Franz, Phys. Rev. 141, 105 (1966).

27. T. Tako, Y. Koga, I. Hirano, and M. Ohi, Jap. J. Appl. Phys. 14, 1641 (1975).

28. N. Kuramochi, H. Fukuyo, I. Matsuda, and N. Shimoi, Jap. J. Appl. Phys. 15, 949 (1976).

29. N. Kuramochi, T. Matsuo, I. Matsuda, and H. Fukuyo, Jap. J. Appl. Phys. 16, 673 (1977).

30. N. Kuramochi, I. Matsuda, and H. Fukuyo, J. Opt. Soc. Am. 68, 1087 (1978).

31. J. Vanier, R. Kunski, P. Pavlin, M. Tetu, and N. Cyr, Can. J. Phys. 60, 1396 (1982).

32. P. Tremblay, N. Cyr, and M. Tetu, Can. J. Phys. (to be published).

33. R. P. Frueholz and J. C. Camparo, J. Appl. Phys. 57, 704 (1985).

34. H. E. Williams, T. M. Kwon and T. McClelland, Proceedings of the 37th Annual Frequency Control Symposium, IEEE Press, New York (1983), p. 12.

35. W. Franzen, Phys. Rev. 115, 850 (1959).

37. F. A. Franz, Phys. Rev. A 6, 1921 (1972).

38. P. Minguzzi, F. Strumia, and P. Violino, Nuovo Cimento 46B, 145 (1966).

39. L. C. Balling, "Optical Pumping," in Advances in Quantum Electronics, Vol. 3, Academic Press, London (1975), p. 1.

40. F. A. Franz and C. H. Volk, Phys. Rev. A 14, 1711 (1976).

41. N. W. Ressler, R. H. Sands, and T. E. Stark, Phys. Rev. 184, 102 (1969).

42. A. Risley and G. Busca, Proceedings of the 32nd Annual Frequency Control Symposium, Electronics Industries Association, Washington, D.C., (1978), p. 506.

43. J. C. Camparo, R. P. Frueholz, and C. H. Volk, Phys. Rev. A 27, 1914 (1983).

44. J. D. Jackson, Classical Electrodynamics, Wiley, New York (1962), p. 256.

45. R. H. Pennington, Introductory Computer Methods and Numerical Analysis, Collier-MacMillan, Canada, Toronto (1970).

46. J. C. Camparo and R. P. Frueholz, Phys. Rev. A 30, 803 (1984).

47. I. Matsuda, N. Kuramochi, N. Shiomi, and H. Fukuyo, Jap. J. Appl. Phys. 16, 391 (1977).

APPENDIX: RESULTS OF COMPLEX CONTOUR INTEGRATION

When extracting the Allan variance from the spectral density of fractional frequency fluctuations, integrals of the form

$$\Lambda(\tau) = \int_0^\infty \frac{f^\alpha}{1 + (f/f_n)^2} \sin^4(\pi\tau f)\ df \qquad (A1)$$

with

$$\alpha = -4,\ -2,\ -1,\ 1,\ 2$$

must be evaluated. Evaluation of these integrals may be performed using complex contour techniques. To facilitate evaluation, $\sin^4(\gamma f)$ was written in terms of complex exponentials. For the even integrands, the contour selected extended from $-R$ to $+R$ along the real axis, with a semicircular indention around origin when required. The contour was closed along the upper half of the circle $|z| = R$ in the complex plane with R ultimately permitted to go to infinity. For odd integrands, the contour was composed of three segments. The first segment extended from $+iR$ to zero along the imaginary axis, with semicircular indentions about singularities. The second segment extended from 0 to $+R$ along the real axis, followed by the third segment, a quarter of the circle $|z| = R$ connecting the other segments. Again R was permitted to go to infinity. In evaluating the integral for $\alpha = -1$, it was found to be expeditious to first differentiate the integrand with respect to $\gamma(=\pi\tau)$, eliminating the singularity at the origin. The resultant integral was evaluated. Indefinite integration with respect to γ was then performed.

The results of this analysis are as follows:

$$\alpha = -4: \quad \Lambda(\tau) = \frac{\pi}{4}\left[\frac{4}{3}(\pi\tau)^3 - \frac{\pi\tau}{f_n^2} + \frac{1}{f_n^3}\left(\frac{e^{-4\pi\tau f_n}}{4} - e^{-2\pi\tau f_n} + 3/4\right)\right] \qquad (A2)$$

$$\alpha = -2: \quad \Lambda(\tau) = \frac{\pi^2\tau}{4} - \frac{\pi}{16f_n}\left(e^{-4\pi\tau f_n} - 4e^{-2\pi\tau f_n} + 3\right) \tag{A3}$$

$$\alpha = -1: \quad \Lambda(\tau) = \frac{1}{4f_n}\left[F(4f_n\pi\tau) - 2F(2f_n\pi\tau)\right] \tag{A4a}$$

with

$$F(c\pi\tau) = \frac{e^{c\pi\tau}}{c}\left[Ei(-c\pi\tau) - e^{-c\pi\tau}Ei(c\pi\tau) + \sum_{n=1}^{A}(-1)^n \sum_{k=1}^{n}\frac{(-1)^k(c\pi\tau)^{n-k}}{n\cdot(n-k)!}\right]$$

$$+ \frac{e^{-c\pi\tau}}{c}\left[Ei(c\pi\tau) - e^{c\pi\tau}Ei(-c\pi\tau) + \sum_{n=1}^{B}\sum_{k=1}^{n}\frac{(c\pi\tau)^{n-k}}{n\cdot(n-k)!}\right]$$

$$-\frac{1}{c}\left(\sum_{n=1}^{A}\frac{1}{n} + \sum_{n=1}^{B}\frac{1}{n}\right) \tag{A4b}$$

for $c\pi\tau < 20$. $Ei(x)$ is the exponential integral function,* and A and B are selected to ensure convergence of the respective sums. When $c\pi\tau > 20$, various asymptotic expansions may be employed in deriving $F(c\pi\tau)$ to yield

$$F(c\pi\tau) = \frac{-2}{c}\left[\ln(c\pi\tau) - \sum_{\substack{k=3 \\ k\ \text{odd}}}^{M}\frac{(k-2)!}{(c\pi\tau)^{k-1}}\right] \tag{A4c}$$

with M selected to ensure series convergence to desired level of accuracy.

When α equals either +1 or +2, the integral of Eq. (A1) is not finite. One way this can be overcome is by limiting the range of integration to a maxmium frequency.* Physically this represents the maximum frequency to which the measurement system responds. An alternative means of addressing this

*Handbook of Mathematical Functions, M. Abramowitz and I. A. Stegun, eds., Dover Publications, Inc. (1965), pp. 227-251.

problem, preserving analytic evaluation of the integrals, is to modify the integrand in such a manner that it goes smoothly to zero above a cutoff frequency f_c. This is carried out by altering Eq. (A1) to give

$$\Lambda(\tau) = \int_0^\infty \frac{f^\alpha}{1 + (f/f_n)^2} \frac{1}{1 + (f/f_c)^2} \sin^4(\pi\tau f)df \qquad (A5)$$

Evaluating Eq. A5 for α = +1 and +2 yields

$$\alpha = +1: \Lambda(\tau) = \frac{(f_c)^2}{16(f_c^2 - f_n^2)} \{G(4\pi f_c\tau) - G(4\pi f_n\tau) - 4[G(2\pi f_c\tau) - G(2\pi f_n\tau)]$$

$$+ 6\ \ell n(f_c/f_n)\} \qquad (A6)$$

with $G(x) = e^{-x}\ Ei(x) + e^{x}\ Ei(-x)$

and

$$\alpha = +2: \quad \Lambda(\tau) = \frac{\pi(f_c)^2}{16(f_c^2 - f_n^2)} [f_c(e^{-4\pi f_c\tau} - 4e^{-2\pi f_c\tau} + 3)$$

$$-f_n\ (e^{-4\pi f_n\tau} - 4e^{-2\pi f_n\tau} + 3)] \qquad (A7)$$

LABORATORY OPERATIONS

The Aerospace Corporation functions as an "architect-engineer" for national security projects, specializing in advanced military space systems. Providing research support, the corporation's Laboratory Operations conducts experimental and theoretical investigations that focus on the application of scientific and technical advances to such systems. Vital to the success of these investigations is the technical staff's wide-ranging expertise and its ability to stay current with new developments. This expertise is enhanced by a research program aimed at dealing with the many problems associated with rapidly evolving space systems. Contributing their capabilities to the research effort are these individual laboratories:

Aerophysics Laboratory: Launch vehicle and reentry fluid mechanics, heat transfer and flight dynamics; chemical and electric propulsion, propellant chemistry, chemical dynamics, environmental chemistry, trace detection; spacecraft structural mechanics, contamination, thermal and structural control; high temperature thermomechanics, gas kinetics and radiation; cw and pulsed chemical and excimer laser development including chemical kinetics, spectroscopy, optical resonators, beam control, atmospheric propagation, laser effects and countermeasures.

Chemistry and Physics Laboratory: Atmospheric chemical reactions, atmospheric optics, light scattering, state-specific chemical reactions and radiative signatures of missile plumes, sensor out-of-field-of-view rejection, applied laser spectroscopy, laser chemistry, laser optoelectronics, solar cell physics, battery electrochemistry, space vacuum and radiation effects on materials, lubrication and surface phenomena, thermionic emission, photosensitive materials and detectors, atomic frequency standards, and environmental chemistry.

Computer Science Laboratory: Program verification, program translation, performance-sensitive system design, distributed architectures for spaceborne computers, fault-tolerant computer systems, artificial intelligence, microelectronics applications, communication protocols, and computer security.

Electronics Research Laboratory: Microelectronics, solid-state device physics, compound semiconductors, radiation hardening; electro-optics, quantum electronics, solid-state lasers, optical propagation and communications; microwave semiconductor devices, microwave/millimeter wave measurements, diagnostics and radiometry, microwave/millimeter wave thermionic devices; atomic time and frequency standards; antennas, rf systems, electromagnetic propagation phenomena, space communication systems.

Materials Sciences Laboratory: Development of new materials: metals, alloys, ceramics, polymers and their composites, and new forms of carbon; nondestructive evaluation, component failure analysis and reliability; fracture mechanics and stress corrosion; analysis and evaluation of materials at cryogenic and elevated temperatures as well as in space and enemy-induced environments.

Space Sciences Laboratory: Magnetospheric, auroral and cosmic ray physics, wave-particle interactions, magnetospheric plasma waves; atmospheric and ionospheric physics, density and composition of the upper atmosphere, remote sensing using atmospheric radiation; solar physics, infrared astronomy, infrared signature analysis; effects of solar activity, magnetic storms and nuclear explosions on the earth's atmosphere, ionosphere and magnetosphere; effects of electromagnetic and particulate radiations on space systems; space instrumentation.

END

DTIC

9—86